Laser diagnostics of Nitric Oxide inside a two-stroke DI Diesel engine

G.G.M. Stoffels†, E.J. van den Boom, C.M.I. Spaanjaars, N. Dam,

W.L. Meerts and J.J. ter Meulen

Applied Physics, University of Nijmegen

†Corresponding author: Mrs. G.G.M. Stoffels

Department of Molecular and Laser Physics

University of Nijmegen

Toernooiveld 1

NL-6525 ED Nijmegen

The Netherlands

Tel. ++31 24 365 3017

Fax ++31 24 365 3311

E-mail: genie@sci.kun.nl

Word count: Total: 5615 words

6 figures = 1200 words

4 equations = 84 words

main body = 4331 words

Main body: Word count of LaTeX file with all LaTeX commands removed (Unix software, 'detex *filename* | wc'). Title page, abstract (150 words) and figure captions not included in word count; references (440 words) are included.

ABSTRACT

The Nitric oxide (NO) content and distribution within the combustion chamber of an optically accessible one-cylinder two-stroke direct-injection Diesel engine have been studied by means of Laser Induced Fluorescence. Using 193 nm excitation of NO, detection of the ensuing fluorescence at 208 nm and 216 nm allows determination of the in-cylinder NO content throughout the whole combustion cycle. Images of the two-dimensional NO distribution in a plane perpendicular to the cylinder axis have been recorded for crank angles larger than 31° after Top Dead Center (aTDC). The transformation of NO fluorescence signal into semi-quantitative in-cylinder NO densities is discussed, with an emphasis on the problem posed by spectroscopic interference of Oxygen fluorescence. It is concluded that, in this engine, the bulk of the NO formation takes place relatively late in the stroke, at crank angles larger than 25° aTDC.

INTRODUCTION

Strategies for the reduction of toxic emissions from Diesel engines focus on particulates (soot) and oxides of Nitrogen (NO_x). Although both of these components are formed during combustion, legislation is concerned only with the exhaust products. Emission control therefore aims at either catalytic exhaust gas aftertreatment or at combustion optimisation, where optimisation is taken to imply reduced toxic compound formation while (at least) maintaining combustion efficiency. Combustion optimisation, arguably the more fundamental way of tackling the emission problem, poses a huge challenge both to experimental data acquisition and interpretation, and to theoretical combustion modelling. This paper intends to contribute to the former aspect. We have used non-intrusive optical diagnostics, based on Laser Induced Fluorescence, to monitor the amount as well as the distribution of Nitric oxide (NO) inside the combustion chamber of a Diesel engine.

Laser based optical diagnostics of combustion processes are appreciated for their ability to combine non-intrusiveness with selectivity for specific chemical species [1]. As such, they have been applied both to open flames [2, 3, 4, 5, 6] and to internal combustion engines [7, 8, 9, 10, 11] Among the manifold of optical techniques available, only Laser Induced Fluorescence (LIF) has the sensitivity to provide instantaneous, two-dimensional (2D) information on minority species distributions in combustion processes. The measurement principle of this planar LIF (PLIF) technique involves electronic excitation of the molecules of interest by a thin sheet of laser radiation, and detection of the subsequent fluorescence in a direction perpendicular to the sheet by an intensified CCD camera. PLIF has been used to demonstrate the presence of a large number of specific small molecules in a variety

of combustion environments (see e.g. [2, 3]), but in general it is very hard to quantify. Although in principle the LIF intensity is linearly proportional to the local number density of laser-excited molecules, the proportionality constant depends on the local physico-chemical environment, involving local temperature, density, chemical composition and possibly spectroscopic interference by other molecules. Since these parameters are usually difficult to assess simultaneously with the (P)LIF measurements, one must have recourse to model assumptions.

The present paper reports LIF and PLIF measurements of the NO density within the combustion chamber of a small, two-stroke direct-injection (DI) Diesel engine, running on standard Diesel fuel. NO fluorescence distributions and dispersed fluorescence spectra are presented as a function of crank angle throughout the whole stroke, and ways towards their semi-quantitative interpretation are discussed.

ENGINE AND OPTICAL SETUP

All measurements are performed on a one-cylinder, two-stroke, DI Diesel engine (Sachs; bore 81 mm, stroke 80 mm, swept volume 412 cc) that has been made optically accessible by mounting quartz (Suprasil I) windows in the cylinder wall as well as centrally in the cylinder head (see fig. 1; W1-3). A flat piston with a shallow slot (0.5 mm depth) in its upper surface was used to provide optical access through the side windows throughout the whole engine cycle. The engine is operated steadily running (1200 rpm) on standard Diesel fuel, obtained from a local retailer, and was loaded by a water-cooled electric brake with up to 3.5 Nm (0.44 kW). Fuel is injected through a three-hole nozzle, located 6 mm above the laser

fig. 1

beam (see below), in a direction perpendicular to the laser beam path. Fuel injection starts at 35° before Top Dead Center (bTDC). The exhaust port opens at 105° after Top Dead Center (aTDC), the inlet ports at 121° aTDC. Inlet air is supplied under an overpressure of typically 0.2 bar to improve scavenging. With a compression ratio of 13, the pressure, P, in the engine follows the curve shown in fig. 2. Combustion is seen to start at 13° bTDC, and a peak pressure of 72 bar is reached slightly after TDC. Natural flame emission can be observed up to about 60° aTDC. Its spectrum can be well fitted to a Planck black body radiation curve, and shows no additional structure at any crank angle, indicating that it is mainly due to light emission by glowing soot particles. The Planck curves can be used to derive a temperature from the natural emission spectrum as a function of crank angle (Θ). These data have been included in fig. 2; details will be published elsewhere [12]. In the figure, the solid line represents the estimated gas temperature based on adiabatic expansion (PV^γ = constant, $\gamma = 1.4$) of an ideal gas during the later part of the stroke. It is matched to the experimental data at intermediate crank angles ($\Theta \approx 20°$ aTDC), on the assumption that here the soot particles will still be small, so that their temperature will represent the local gas temperature fairly well. At larger crank angles the gas is expected to cool down faster than the more voluminous soot particles, causing the natural emission spectrum to overestimate the actual gas temperature.

fig. 2.

All (P)LIF measurements on NO employed a pulsed, tunable ArF excimer laser (Λ Physik Compex 350T; $\lambda = 192.9 - 193.9$ nm, bandwidth ≈ 0.7 cm^{-1}, 20 nsec pulse duration) to excite NO on the $R_1(23.5)$ or the $R_1(26.5)$ transition of the $D^2\Sigma^+(v' = 0) \leftarrow X^2\Pi(v'' = 1)$ band. The laser is synchronised to the engine cycle with a precision of $< 0.6°$ crank angle. It emits a beam with rectangular cross section, which, for all measurements in which the

combustion was illuminated through the side window, is focussed down to a sheet of about 0.1 mm thickness inside the engine. The beam traverses the combustion chamber in a plane perpendicular to the cylinder axis (see fig. 1), and is located within the slot in the piston upper surface when the piston is at TDC. Fluorescence of NO (and also the laser radiation resonantly scattered off small particles (Mie scattering)) is detected through the top window (25 mm diameter; fig. 1) by a 576×384 pixels CCD camera (14 bits dynamic range) equipped with an image intensifier (Princeton Instr. ICCD-576G/RB-E) and a quartz $f/4.5$ 105 mm objective (Nikon). The laser illuminates the whole area beneath the top window, resulting in a measurement volume of 25×0.1 mm (diameter $\times$ thickness).

For the purpose of recording NO fluorescence distributions the fluorescence is recorded through a 4-plate reflection filter, tuned to 208 nm center wavelength with a bandwidth of 5 nm (FWHM). At this setting, the filter is centered on the NO $\mathrm{D}(v' = 0) \rightarrow \mathrm{X}(v'' = 3)$ fluorescence band. Mie scattering images were obtained in the same setup, but with the filter mirrors replaced by broad-band aluminium mirrors. Alternatively, the camera may be mounted behind an imaging monochromator (Chromex 250IS) with a 1200 gr/mm holographic grating blazed at 250 nm, as part of an Optical Multichannel Analyser (OMA) setup, to spectrally disperse the fluorescence. For all fluorescence measurements the image intensifier was used with a gate width of 50 nsec, which was sufficient to collect all LIF (no signal increase for longer gate times) while keeping the contribution of the natural flame emission down to a manageable (and usually negligible) level. The latter was, however, always measured separately and subtracted from the LIF data.

DATA EVALUATION

Even though qualitative data on chemical species distributions within a combustion environment are of interest in themselves, one of the goals of our present research is to quantify the LIF data as much as possible. This will allow them to be compared throughout the stroke and for different engine operating conditions, different fuels and fuel injection systems, and so on. The LIF yield will be described using a model in which the energy level structure of NO is simplified to a 3-level system coupled to a 'bath' of all other levels by collisional energy transfer processes. Rotational energy transfer in the ground state [13] will be neglected, because of the low laser intensity within the engine. For the general case of pulsed LIF in which all fluorescence out of the laser-excited state is recorded, the fluorescence yield $S_{\mathrm{LIF}}(x,y)$ due to a local NO density $\rho_{\mathrm{NO}}(x,y)$ can be written as

$$S_{\mathrm{LIF}}(x,y) = \wp I_{\mathrm{L}}(x,y) g(\nu_{\mathrm{L}},\nu_0) f_{vJ}(T) \rho_{\mathrm{NO}}(x,y) \frac{\mathcal{A}}{\mathcal{A}+Q} \,, \tag{1}$$

in which x and y are the spatial coordinates within the plane illuminated by the laser and $\wp$ is a proportionality constant including experimental parameters like optics collection efficiency, camera sensitivity, absorption line strength, etc. $I_{\mathrm{L}}(x,y)$ denotes the local laser beam intensity and $g(\nu_{\mathrm{L}},\nu_0)$ is the overlap integral of the laser line profile with the NO absorption spectrum. Lacking data on the pressure broadening and shift of transitions in the $\mathrm{D}(v'=0) \leftarrow \mathrm{X}(v''=1)$, and considering that several transitions will contribute to the absorption at increasing pressure, we have taken the latter constant for the present. The temperature-dependent fractional population of the probed rovibrational state is described by the Boltzmann fraction $f_{vJ}(T)$ and the fluorescence yield is determined by the Stern-Vollmer factor $\mathcal{A}/(\mathcal{A}+Q)$, in which $\mathcal{A}$ denotes the spontaneous emission rate on the vibronic

transition that is monitored and Q denotes the effective non-radiative decay rate. The non-radiative decay processes that reduce the fluorescence yield are a result of intermolecular collisions and include both Electronic Energy Transfer (EET; notably D $\rightarrow$ A and D $\rightarrow$ C) and quenching (D $\rightarrow$ X).

In order to extract the NO density from the LIF signal S_{LIF}, all other factors in eq. 1 have to be known. Most of these factors depend on position (x, y) and/or on engine operating conditions, and can therefore not be calibrated by *e.g.* an exhaust gas measurement. Those factors that are particularly difficult to evaluate are discussed individually below.

Local laser intensity $I_{\mathrm{L}}(x, y)$: The laser intensity suffers severe attenuation on its way through the combustion chamber. At larger crank angles (*i.e.* later in the stroke) this attenuation is expected to be caused mainly by scattering off and absorption by particulates, whereas at smaller crank angles absorption by still unburned fuel will also contribute [14]. An independent measure of the local laser intensity is provided by Mie scattering, here understood to comprise elastic light scattering off small particles (regardless of their size). On the assumption *i*) that the laser intensity attenuation is mainly due to scattering off and absorption by small particles (oil, soot, fuel droplets) and *ii*) that there exists a linear relationship between scattering and absorption cross sections of these particles [15], the local laser intensity can be reconstructed from measurements of the local Mie scattered intensity combined with overall transmission measurements. Details of the reconstruction method will be published elsewhere [16]; data on the overall transmission of 193 nm light through the engine are included in fig. 2. The rise in transmission around 60° aTDC coincides with the end of the visible combustion, suggesting that unburned fuel indeed plays an important part in absorption of 193 nm laser radiation (see also [14]).

Stern-Vollmer factor $\mathcal{A}/(\mathcal{A}+Q)$: The spontaneous emission rate on the D($v'=0$) $\rightarrow$ X(v'') transition can be estimated from the radiative lifetime of the D-state ($\tau = 18$ nsec [17]) and the appropriate Franck-Condon factor (0.165 for $v''=3$, calculated using the approximation by Nicholls [18] and molecular data from Huber & Herzberg [19]), yielding $\mathcal{A}_{03} = 9.2{\cdot}10^6$ sec^{-1}. The non-radiative decay rate Q poses a more serious problem. Although there is a considerable amount of data available for the NO A-state quenching, data for the D-state are all but lacking. Preliminary results of measurements on the D-state fluorescence yield under conditions of elevated temperature and pressure indicate that D $\rightarrow$ A EET by collisions with N_2 provide a very efficient decay channel [20]. For the present purpose, we have simply assumed

$$Q = \bar{v}_{\mathrm{rel}}\rho\sigma \gg \mathcal{A} = \mathcal{A}_{03} \ , \tag{2}$$

with $\bar{v}_{\mathrm{rel}} = (8kT/\pi\mu)^{1/2}$ the relative velocity between collision partners, ρ the total number density and σ an effective quenching cross section taken to be independent of pressure and temperature.

In summary, using the above assumptions the local NO number density can be extracted from PLIF images and dispersed fluorescence spectra as

$$\rho_{\mathrm{NO}}(x,y) \propto \frac{PT^{-1/2}}{g(\nu_{\mathrm{L}},\nu_0)f_{vJ}(T)}\frac{S_{\mathrm{LIF}}(x,y)}{I_{\mathrm{L}}(x,y)} \ , \tag{3}$$

where I_{L} is reconstructed from separately recorded Mie scattering images as discussed above. Assuming the average NO density in an image or spectrum to also represent the average density in the whole cylinder, the total amount of NO can be written as

$$\mathcal{N}_{\mathrm{NO}} \propto V_{\mathrm{cyl}} \int_{\mathrm{image}} \rho_{\mathrm{NO}}(x,y)\mathrm{d}x\mathrm{d}y \ , \tag{4}$$

in which V_{cyl} is the in-cylinder volume (depends on crank angle).

RESULTS AND DISCUSSION

Dispersed Fluorescence Spectra

Figure 3 shows dispersed fluorescence spectra (averaged over 250 engine cycles) for different crank angles, recorded with the OMA system (100 μm entrance slit) and illuminating the combustion through the side entrance window (fig. 1). The excitation laser frequency was set to the $R_1(23.5)$ NO transition at 51656 cm^{-1} [21]. A normal incidence 193 nm laser mirror was used in front of the collection optics to suppress Mie scattered radiation. Spectral structure can be identified for crank angles $\Theta \gtrsim 25°$ aTDC, and all features can be attributed to NO fluorescence. The most prominent features (at 208, 216 and 225 nm) arise from fluorescence out of the laser-excited D-state ($D(v' = 0) \rightarrow X(v'' = 3, 4, 5)$ bands; the $0 \rightarrow 2$ band at 201 nm is suppressed by the 193 nm mirror). Also present are fluorescence bands originating from the $C(v' = 0)$-state (bands at 204, 212 and 220 nm) and probably from the $A(v' = 0)$-state (shoulder at 225 nm), that are indirectly excited through collisional EET out of the D-state. The fluorescence intensities are seen to remain rather constant for $\Theta \gtrsim 45°$ aTDC, although the relative intensities of the D and C bands change slightly, indicating the variation of collisional energy transfer efficiency during the stroke. Since both the Mie scattering intensity and the overall laser beam transmission (fig. 2) are very low near TDC, the lack of spectral structure for $\Theta \lesssim 25°$ aTDC is probably due to the lack of laser intensity. Similar observations have been reported recently by Sick [14].

fig. 3

The attenuation problem can be circumvented by coupling the excitation laser into the combustion chamber through the top window, so that it directly enters the combustion chamber within the observation area (see fig. 1). Dispersed fluorescence spectra (averaged

over 100 engine cycles) recorded using this optical setup, excitation on the $R_1(26.5)$ NO transition at 51713 cm^{-1} [21] and a monochromator entrance slit of 50 μm, are presented in fig. 4. All these spectra show a persistent peak at 207.8 nm, which, however, is an unfortunate artefact caused by laser induced phosphorescence of the quartz observation window; it shows up in these spectra because laser excitation and LIF observation now occur through the same window. More informative is the fact that all spectra, also those around TDC, show structure. This indicates that laser intensity is available in the combustion chamber even at small crank angles. The spectral structure shows a considerable qualitative change around 30° aTDC. For $\Theta \lesssim 30°$ aTDC two prominent fluorescence features are found at 211 and 217.5 nm, the latter with a persistent doublet structure even at TDC (where $P = 72$ bar, $T \approx 2800$ K; see fig. 2). Both features can be ascribed to Oxygen (O_2) fluorescence [22]. For $\Theta \gtrsim 30°$ aTDC these O_2 features disappear and are replaced by somewhat broader spectral structures around 208 nm (red shoulder on the quartz phosphorescence peak) and 216 nm (and also two low humps at 212.5 and 220 nm). These structures can all be attributed to NO, and correspond to the dispersion peaks of fig. 3. Even though the NO fluorescence is most evident in the spectra for $\Theta \gtrsim 30°$ aTDC, it should be stressed that NO fluorescence can be recognized in all spectra for $\Theta \geq$ TDC. The integrated fluorescence signal of the $D(v' = 0) \rightarrow X(v'' = 4)$ band at 216 nm (right at the blue side of the O_2 band at 217.5 nm and clearly visible in the spectra for $\Theta = 25°$ aTDC and $\Theta = 31°$ aTDC) is plotted in the uppermost panel of fig. 4. Note that these signal strengths have not been corrected for anything, and just present raw data. Fluorescence bands of NO and O_2 coincide in the 225 nm region, which is the reason why the spectrum in this wavelength region is relatively invariant. The shape of the 225 nm band does, however, change from a multiple-peaked

fig. 4

structure (characteristic for O_2, due to strong predissociation of the upper state [23]) for $\Theta \lesssim 30°$ aTDC to a structureless bump (characteristic for NO) at $\Theta \gtrsim 30°$ aTDC.

Two-dimensional NO distributions

The spectra shown in figs. 3 and 4 have some consequences for PLIF measurements that aim at recording 2D NO distributions. Excitation-emission spectra recorded in the two-stroke engine at $\Theta = 43°$ aTDC have shown that all strong NO transitions (within the ArF laser tuning range) lie close to some O_2 resonance, so that efficient excitation of NO unavoidably also involves some overlap with an O_2 transition within the laser bandwidth [20, 24, 25, 26]. Evidently, since O_2 excitation can not completely be avoided, the NO band(s) should be filtered out of the total fluorescence. In our case, the $D(v' = 0) \rightarrow X(v'' = 3)$ NO fluorescence band at 208 nm was used for imaging, because it lies relatively isolated from O_2 fluorescence bands (nearest neighbours observed at 205 nm and 211 nm), and is also sufficiently distant from the excitation wavelength to avoid contributions of Mie scattered laser radiation. Unfortunately, this detection wavelength exactly coincides with the laser induced phosphorescence peak in the quartz observation window (see fig. 4), which, for the moment, precludes using illumination through the observation (top) window.

Figure 5 presents false colour NO distributions at several crank angles. These images are fig. 5 based on NO fluorescence distributions, illuminating the combustion with a thin light sheet (excitation on the $R_1(23.5)$) through the side entrance window and detecting a 5 nm wide fluorescence band centered at 208 nm through the top window. The LIF distributions were averaged over 25 engine cycles, and are corrected only for the local laser intensity by the method briefly discussed above. To the extent that quenching and other collisional energy

transfer processes are, at least on average, uniform over the field of view, the images of fig. 5 represent NO distributions in arbitrary units (that is, the local pixel values are proportional to the local NO density). Since they are individually scaled to enhance contrast, only the distributions should be compared, not the intensities.

For $\Theta \lesssim 35°$ aTDC the NO fluorescence signal is weak, and, since at these crank angles the Mie scattering images used for reconstruction of the local laser intensity may contain a contribution from the flame luminosity, the fluorescence distribution is hard to interpret. At larger crank angles the signal level improves considerably. The formation of NO is seen to be concentrated in the leftmost part of the observation area, slowly spreading into a more uniform distribution as the crank angle increases. At 142° aTDC, when both inlet and outlet ports are open, a uniform distribution of the remaining NO is seen. (Note that the plane of observation is located high in the cylinder, whereas the scavenging ports are located near BDC.) Since also the distribution of scattering particles is concentrated in the lefthand part of the observation region (data not shown), the images point to the occurrence of a reproducible flow pattern inside the cylinder of this engine.

The in-cylinder NO content

Both the dispersed fluorescence spectra of fig. 3 and the integrated pixel values of the images of fig. 5 can be processed according to the prescriptions discussed above (Data evaluation section), to arrive at a measure for the NO density as a function of crank angle (eqs. 3 and 4). This procedure cannot yet be applied to the data of fig. 4, because the current setup does not allow transmission measurements in a top window illumination setup. Figure 6 presents curves that are proportional to the NO content within the cylinder, obtained from

Fig 6.

evaluation of the data in figs. 3 and 5. They show a steep rise starting at $\Theta \approx 20°$ aTDC and reach a maximum around 45° aTDC followed by a more gradual decline during the later part of the stroke. Similar curves have been measured in several different runs, as well as for various engine operating conditions and fuels, and are found to reproduce well. However, in view of the uncertainties involved in some of the factors occurring in eq. 1, some systematical error may still be present in the curves. The curves in fig. 6 show that, in this particular engine, the bulk of NO formation takes place relatively late in the stroke, with the premixed combustion and early mixing-controlled combustion phases [27] contributing only little. This result, qualitatively born out by the spectra in fig. 4 also, is in agreement with theoretical predictions by the group of Peters [28]. They also agree with recent results from the Sandia [29] and Mitsubishi [30] combustion research groups, although there, in the absence of spectral data, the possibility of O_2 fluorescence interference cannot unequivocally be excluded.

From the NO curves of fig. 6 it seems that the high-temperature reactions of the Zel'dovich reaction mechanism [31], which would predict the bulk of NO formation to take place during the high temperature phase of the combustion (that is, around TDC), play only a minor role. This may be rationalized by considering the possibility that the high temperatures reached during the early combustion are achieved only locally, in regions of fast combustion (*e.g.* at the evaporating edges of fuel droplets), and that the Oxygen is consumed there by combustion rather than being involved in NO formation.

A second conspicuous feature of the NO curves in fig. 6 is their decline towards larger crank angles. There may be several explanations for this effect. Nitric oxide is chemically not particularly stable, and will be converted to NO_2 during the colder part of the stroke.

(Note that Diesel engines operate under lean conditions, so there will be O_2 left after the combustion has subsided; see e.g. [27].) This would lead to a reduction of the NO content in the engine, which has, in fact, been predicted by calculations [28], albeit not to the extent observed in fig. 6. Another, but elusive, explanation may be found in NO chemistry on the surface of soot particles that are also produced in large amounts during the combustion in this particular engine. This, however, is a subject of which little is known. Finally, a systematic measurement error may be involved, if gas flow in the cylinder is such that the formed NO is confined spatially to some kind of cloud that is transported out of the region probed by the excitation laser. If this were to be the case, it would be better to concentrate on densities (eq. 3) rather than on total amounts (eq. 4).

CONCLUSION

The NO formation within the combustion chamber of a DI Diesel engine operated on standard Diesel fuel has been studied throughout the whole engine cycle using ArF excimer laser induced fluorescence. LIF images visualise the two-dimensional NO distribution in a plane located 6 mm below the fuel injector. Dispersed fluorescence spectra have been used to obtain a semi-quantitative measure (up to a calibration constant) for the amount of NO present in the cylinder at any crank angle, and the post-processing procedures that must be used to extract these data from the LIF signal strength are discussed. The results for this particular engine show a relatively late start of the NO formation at about 20° aTDC. The NO content reaches a maximum at about 45° aTDC after which it gradually decreases.

Our results show the feasibility of obtaining semi-quantitative data on the NO distribu-

tion in a fairly realistic Diesel engine by means of ArF laser diagnostics. Great care must be taken to avoid spectroscopic interference of, particularly, Oxygen. In order to arrive at these data, a number of assumptions has had to be made, the substantiation of which has to be part of future research. Notably, this concerns *i*) information on collisional energy transfer involving both the ground state (RET) and the electronically excited $D^2\Sigma^+$-state (EET) for different collision partners, *ii*) data on pressure broadening and shifting of NO absorption lines and *iii*) methods to assess the local in-cylinder laser intensity.

Acknowledgements

It is a pleasure to acknowledge the expert technical assistance of especially L. Gerritsen and P. van Dijk of the workshop of the University of Nijmegen, as well as the help of E. van Leeuwen during the build-up phase of the project. This research is supported by the Technology Foundation (STW), the Netherlands Organization for Applied Scientific Research (TNO) and Esso.

References

[1] Eckbreth, A.C., *Laser diagnostics for combustion temperature and species*, Abacus Press, Tunbridge Wells, UK, 1988.

[2] Klein-Douwel, R.J.H., Spaanjaars, J.J.L. and ter Meulen, J.J., *J. Appl. Phys.* 78: 2086-2096 (1995).

[3] Rothe, E.W. and Andresen, P., *Appl. Opt.* 36: 3971-4033 (1997).

[4] Vyrodov, A.O., Heinze, J., Dillmann, M., Meier, U.E. and Stricker, W., *Appl. Phys. B* 61: 409-414 (1995).

[5] Reisel, J. and Laurendeau, N.M., *Energy & Fuels* 8: 1115-1122 (1994).

[6] Reisel, J.R., Carter, C.D. and Laurendeau, N.M., *Combust. Flame* 92: 485-489 (1993).

[7] Espey, C. and Dec, J., *SAE paper* 930971: 1-21 (1993).

[8] Knapp, M., Luczak, A., Schlüter, H., Beushausen, V., Hentschel, W. and Andresen, P., *Appl. Opt.* 35: 4009-4017 (1996).

[9] Alataş, B., Pinson, J.A., Litzinger, T.A. and Santavicca, D.A., *SAE paper* 930973: 1-11 (1993).

[10] Brugman, T.M., Klein-Douwel, R., Huigen, G., van Walwijk, E. and ter Meulen, J.J., *Appl. Phys. B* 57: 405-410 (1993).

[11] Brugman, T.M., Stoffels, G.G.M., Dam, N., Meerts, W.L. and ter Meulen, J.J., *Appl. Phys. B* 64: 717-724 (1997).

[12] Stoffels, G.G.M. *et al.*, in preparation.

[13] Rothe, E.W., Gu, Y.W. and Reck, G.P., *Appl. Opt.* 35: 934-947 (1996).

[14] Sick, V., in Leipertz, A. (ed.), *Berichte zur Energie- und Verfahrenstechnik*, Heft 97.1, ESYTEC GmbH, Erlangen (Germany), 1997, pp 177-190.

[15] Bohren, C.F. and Huffman, D.R., *Absorption and scattering of light by small particles*, Wiley, New York, 1983.

[16] Stoffels, G.G.M. *et al.*, in preparation.

[17] Radzig, A.A. and Smirnov, B.M., *Reference data on atoms, molecules and ions*, Springer Verlag, Berlin, 1985.

[18] Nicholls, R.W., *J. Chem. Phys.* 74: 6980-6981 (1981).

[19] Huber, K.P. and Herzberg, G., *Molecular spectra and molecular structure IV. Constants of diatomic molecules*, van Nostrand Reinhold, New York, 1979.

[20] van den Boom, E.J. *et al.*, in preparation.

[21] Versluis, M., Ebben, M., Drabbels, M. and ter Meulen, J.J., *Appl. Opt.* 30: 5229-5232 (1991).

[22] Wodtke, A.M., Huwel, L., Schlüter, H., Voges, H., Meijer, G. and Andresen, P., *J. Chem. Phys.* 89: 1929-1935 (1988).

[23] Andresen, P., Bath, A., Lülf, H.W., Meijer, G. and ter Meulen, J.J., *Appl. Opt.* 27: 365-378 (1988).

[24] Shimauchi, M., Miura, T. and Takuma, H., *Jpn. J. Appl. Phys.* 33: 4628-4635 (1994).

[25] Kruppenie, P.H., *J. Chem. Phys. Ref. Data* 1: 423-534 (1972).

[26] Lee, M.P. and Hanson, R.K., *J. Quant. Spectrosc. Radiat. Transf.* 36: 425-440 (1986).

[27] Heywood, J.B., *Internal Combustion Engine Fundamentals*, McGraw-Hill, Singapore, 1988.

[28] Pitsch, H., Barths, H. and Peters, N., in Leipertz, A. (ed.), *Berichte zur Energie- und Verfahrenstechnik*, Heft 97.1, ESYTEC GmbH, Erlangen (Germany), 1997, pp 139-163.

[29] Dec, J., *Sandia newsletter*, sept./oct. 1997 (unpublished).

[30] Nakagawa, H., Endo, H., Deguchi, Y., Noda, M., Oikawa, H. and Shimada, T., *SAE paper* 970874: 187-196 (1997).

[31] Warnatz, J., Maas, U. and Dibble, R.W., *Combustion*, Springer Verlag, Berlin, 1996.

Figure captions

Figure 1

Schematical view of the optically accessible Diesel engine and the optical setup. The excimer laser beam (ArF) either traverses the combustion chamber (as a thin sheet parallel to the piston upper surface) through the two side windows (W1 and W2), or it is used unfocussed to illuminate the combustion through the top window (W3). Fluorescence (or natural flame emission) is observed through the top window by an intensified CCD camera (ICCD) positioned behind either a narrow-band reflection filter (used for imaging) or a monochromator (used for fluorescence dispersion) (F).

Figure 2

Parameters of the engine running steadily on standard Diesel fuel. The lower panel shows the in-cylinder pressure and temperature. The solid bar indicates the fuel injection time, and the start of combustion is indicated by CS. Solid squares indicate temperatures derived from the flame emission spectrum (black body radiation; see text); the solid curve is based on calculations assuming adiabatic expansion of an ideal gas during the later part of the stroke. The upper panel shows the transmission of 193 nm radiation through the running engine (note logarithmic scale on ordinate), relative to the transmission at BDC (0.12%); the solid line merely serves as a guide for the eye.

Figure 3

Dispersed fluorescence spectra of NO for different crank angles (° aTDC, indicated at the right), obtained by illuminating the combustion through the side entrance window. All

spectra are to the same scale. Peak identification is provided at the top of the figure (upper electronic state (US); vibrational level in the lower electronic state (LS v'')). See text for details.

Figure 4

Dispersed fluorescence spectra of NO for different crank angles (° aTDC, indicated at the right), obtained by illuminating the combustion through the top window. All spectra are to the same scale. For identification of the NO spectral features, see fig. 3. The increasing intensity at the blue end of the spectra is due to directly scattered laser light, which in this case is much stronger than with side window illumination. The persistent peak at 207.8 nm is due to quartz phosphorescence. The upper panel shows the uncorrected integrated intensity of the NO fluorescence band at 216 nm as a function of crank angle. Opening of the exhaust port is indicated by the black bar.

Figure 5

Images of the NO distribution, averaged over 25 engine cycles, in a plane inside the cylinder, located 6 mm below the fuel injection nozzle. Crank angles are indicated in each image. Images are in a false colour scale, red indicating relatively high density, blue and black relatively low densities. The laser beam travels from right to left, and fuel is injected from the bottom of the images upwards. All images are individually scaled to enhance contrast.

Figure 6

The amount of NO within the combustion chamber as a function of crank angle. The curves are derived from the dispersed fluorescence spectra of fig. 3 (solid squares) and the images

of fig. 5 (open circles), processed along the lines discussed in the data evaluation section of the text.

Figure 1
GGM Stoffels et al.

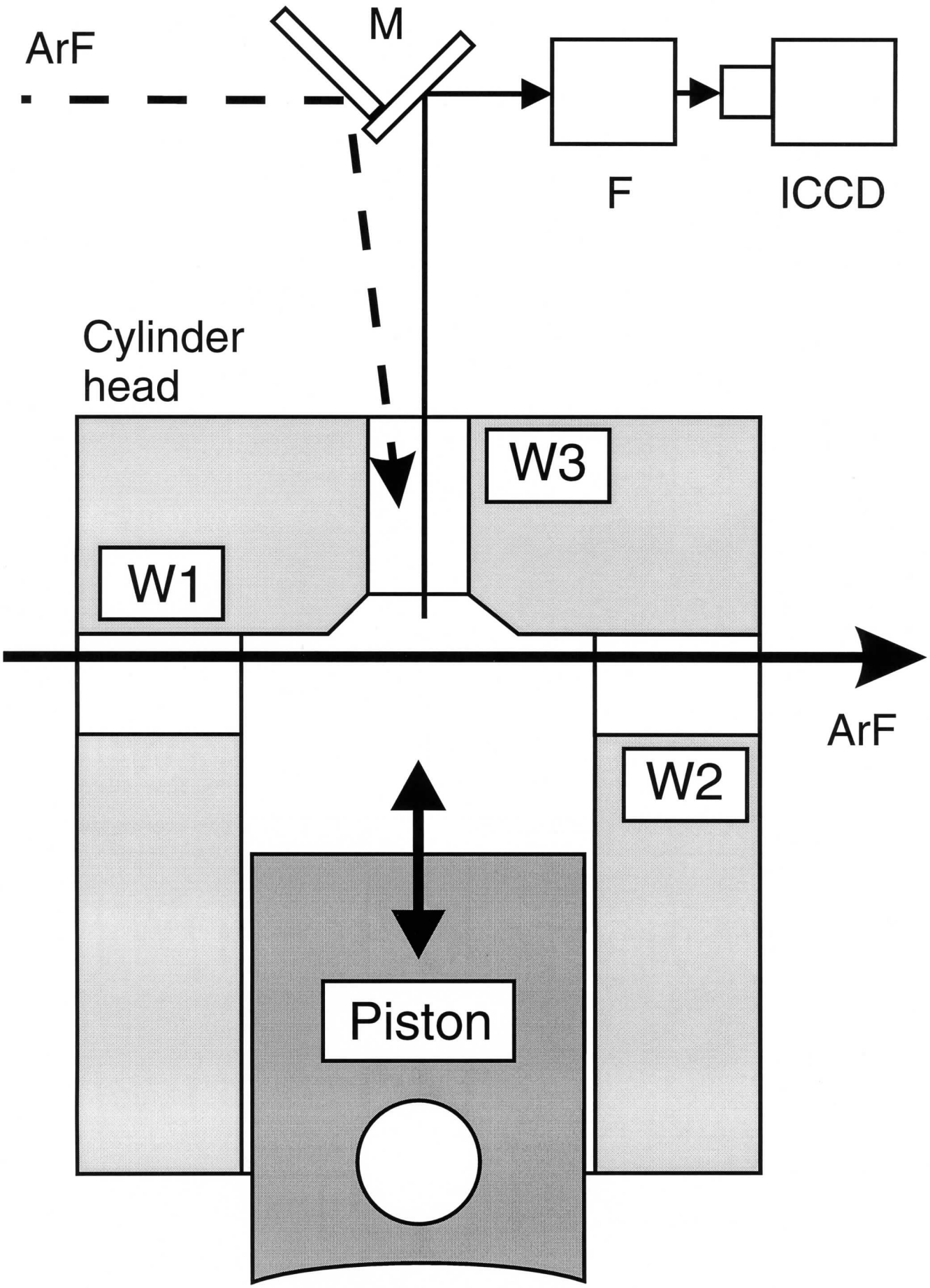

Figure 2
GGM Stoffels et al

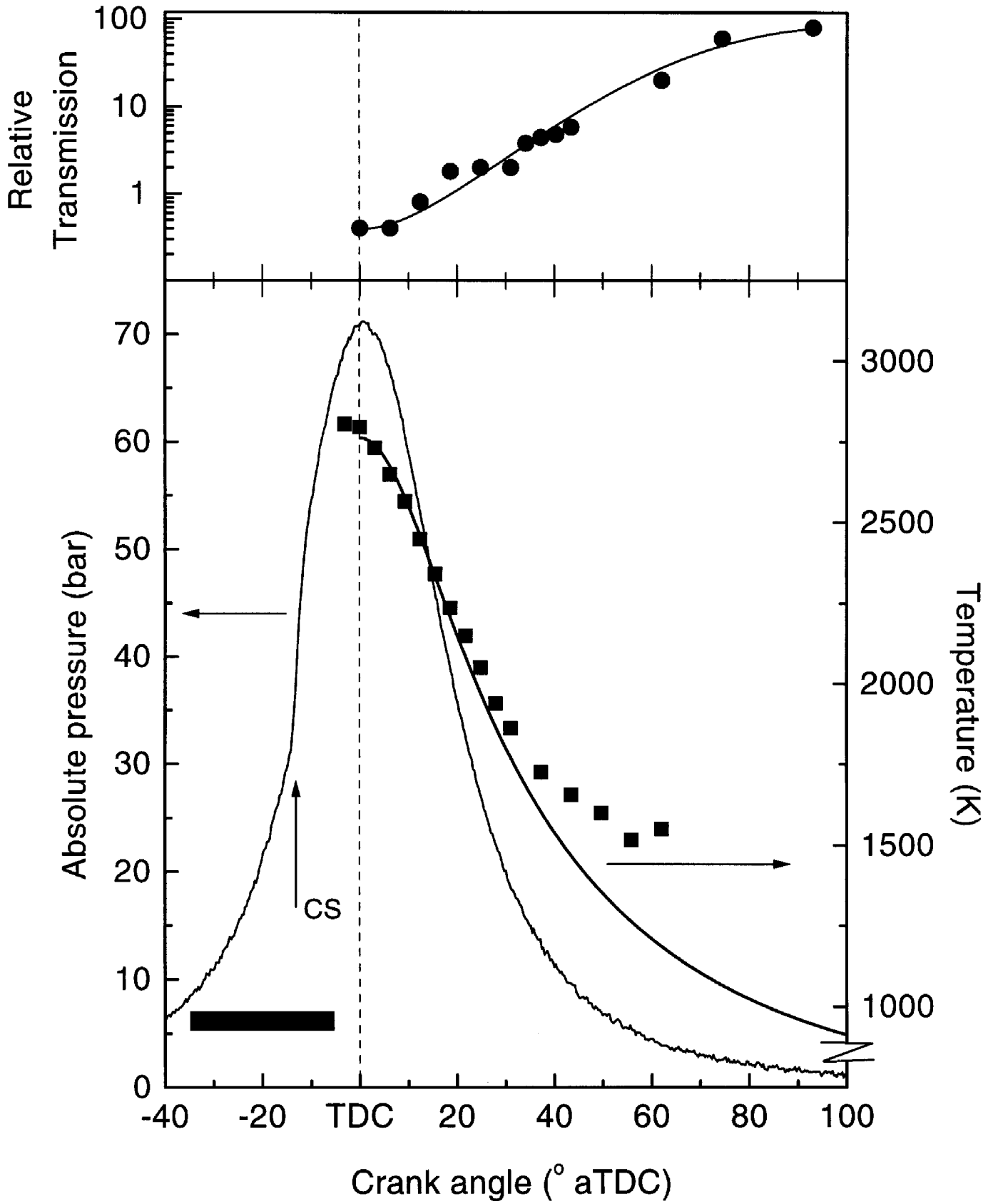

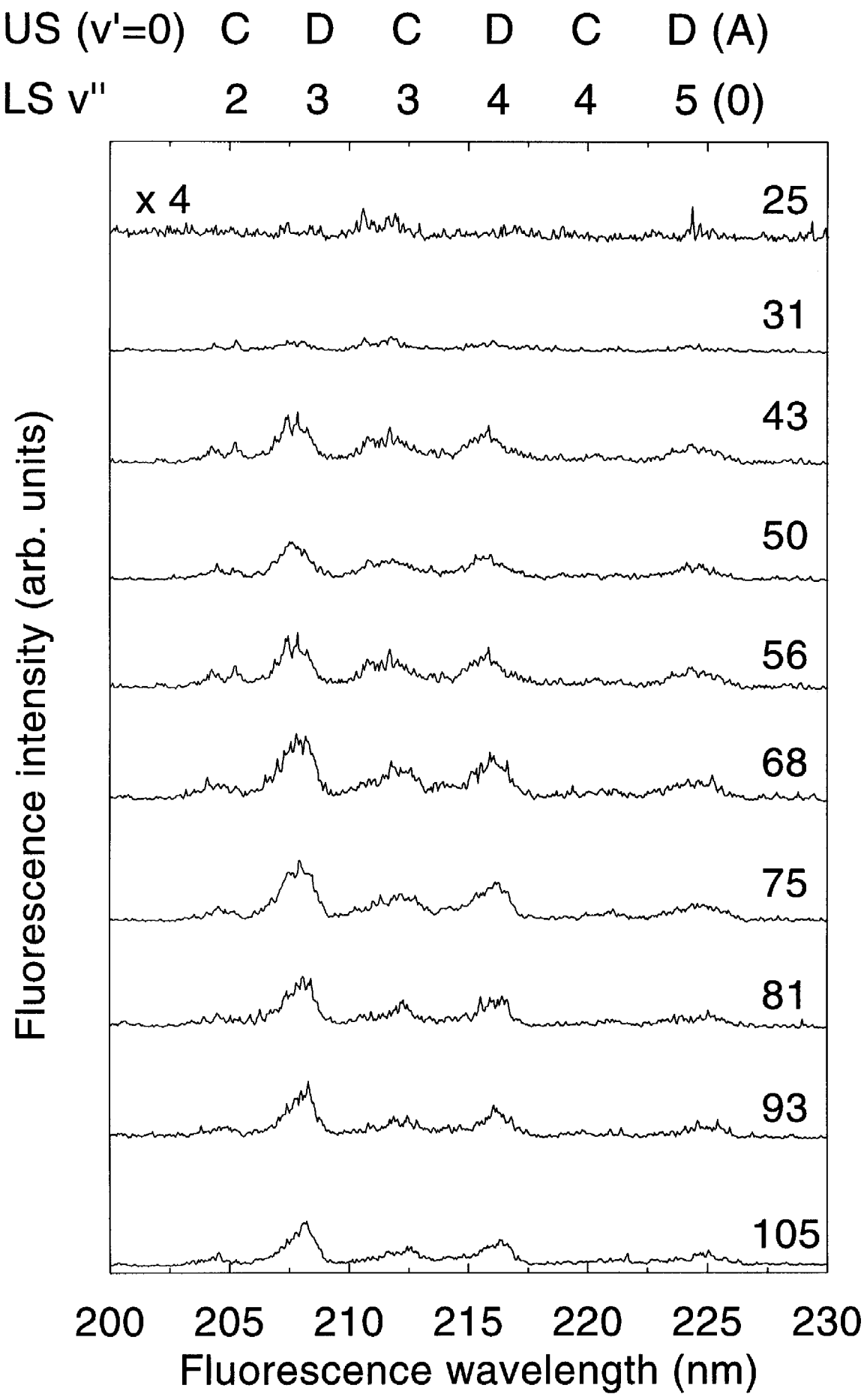

Figure 3

GGM Stoffels et al

Figure 4
GGM Stoffels et al.

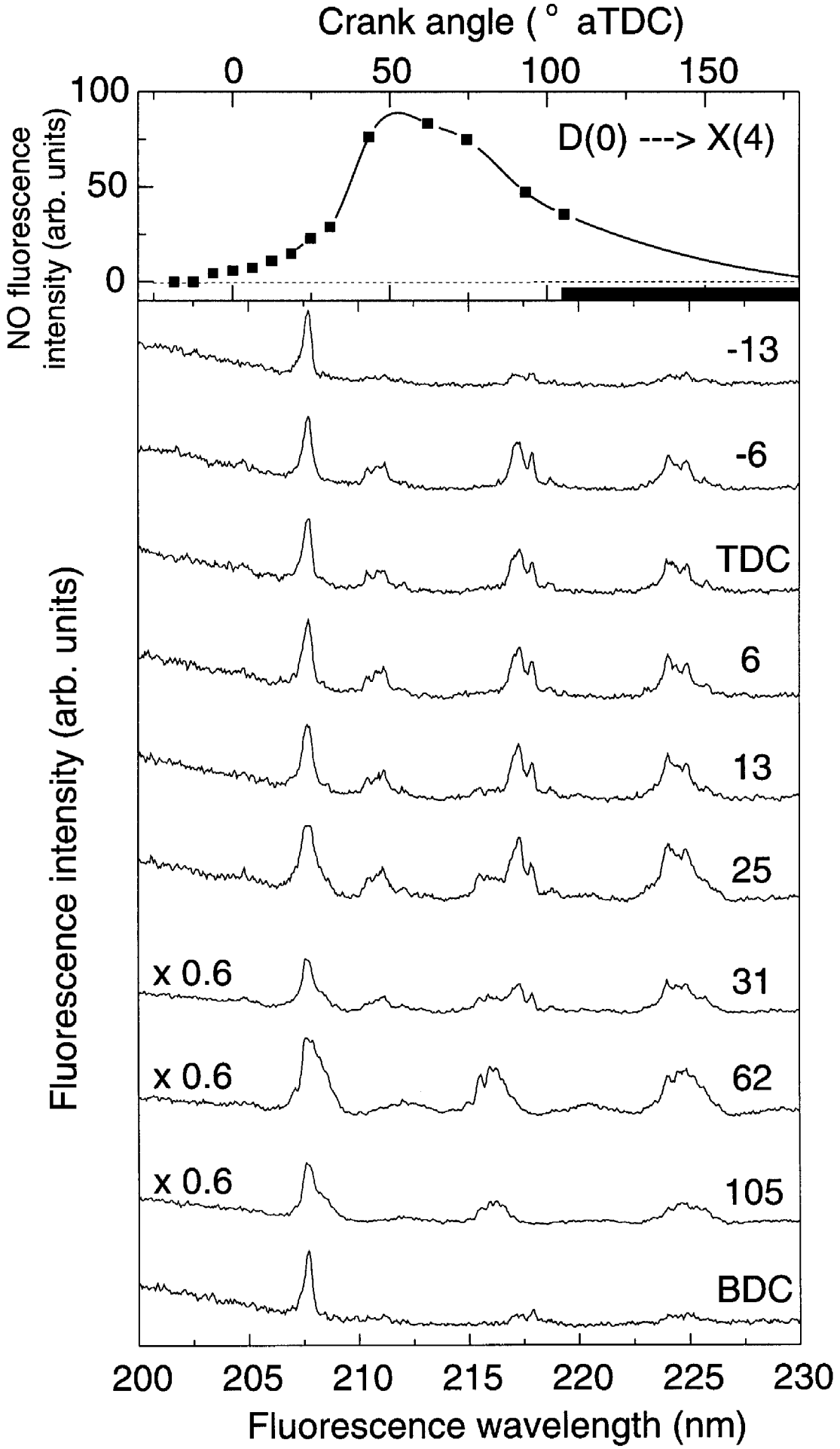

Figure 6
GGM Stoffels et al.